Available online at www.sciencedirect.com
SCIENCE DIRECT®
Journal of Catalysis 225 (2004) 288–299
JOURNAL OF CATALYSIS
www.elsevier.com/locate/jcat

Structural studies of catalytically stabilized model and industrial-supported hydrodesulfurization catalysts

Myriam Perez De la Rosa,[a,*] Samuel Texier,[b] Gilles Berhault,[b,1] Alejandra Camacho,[c] Miguel José Yácaman,[c] Apurva Mehta,[d] Sergio Fuentes,[e] Jorge Ascension Montoya,[f] Florentino Murrieta,[f] and Russell R. Chianelli [a]

[a] *Materials Research Technology Institute, University of Texas at El Paso, El Paso, TX 79968, USA*
[b] *Laboratoire de Catalyse en Chimie Organique, UMR65O3-CNRS, Université de Poitiers, 40 avenue du Recteur Pineau, 86000 Poitiers, France*
[c] *Department of Chemical Engineering and Center for Nano and Molecular Science and Technology, University of Texas at Austin, Austin, TX 78712, USA*
[d] *Stanford Synchrotron Radiation Laboratory, Stanford University, Menlo Park, CA 94025, USA*
[e] *Centro de Ciencias de Ia Materia Condensada, 22830, Ensenada, B.C., Mexico*
[f] *Instituto Méxicano del Pétroleo, Eje Central Cárdenas 152, 07730 Mexico DF, Mexico*

Received 30 January 2004; revised 30 March 2004; accepted 31 March 2004

Available online 25 May 2004

Abstract

The high anisotropic character and inherent disorder in the structure of supported MoS_2-based catalysts that are used extensively to perform hydrotreating reactions for the removal of heteroatoms (S, N, and O), aromatics, and metals make characterization of the active catalyst a difficult challenge. XAS (X-ray absorption spectroscopy), XRD (X-ray diffraction), and HRTEM (high-resolution transmission electron microscopy) have been widely used in an attempt to understand the structure and origin of the active phase in these catalysts. However, all these techniques have limitations in determining the structure of the active MoS_2 phase and the associated Co promoter when used individually. Current techniques are not able to provide information of both lateral dimensions along the basal direction and of stacking height of MoS_2 slabs without ambiguity. We report here the use of a synchrotron source for X-ray-scattering measurements of supported MoS_2 and cobalt-promoted MoS_2 catalysts. This synchrotron source strongly increases the signal to noise ratio resulting in the detection of diffraction features providing information on the dispersion of the active phase. Synchrotron X-ray measurements in combination with HRTEM can then give a more complete picture of catalyst structure and of the active phases present. Furthermore, supported industrial catalysts that have operated under refinery conditions for more than four years have been studied to better understand the stabilized catalytic phase under these conditions. Industrial hydrotreating conditions induce a "destacking" process resulting in the stabilization of single-layered MoS_2-like nanoparticles. This effect has been confirmed on a freshly sulfided model $CoMo/Al_2O_3$ catalyst that underwent substantial morphological change leading to the formation of single slabs under HDS conditions. Other structural effects are also reported. This study emphasizes the importance of determining the catalytically stabilized phases under operating hydrotreating conditions as a basis for understanding the activity and selectivity of this class of catalysts.

Keywords: Molybdenum sulfide; Hydrodesulfurization; CoMo; Stacking; Morphology; X-ray scattering

1. Introduction

Faced with heavier crudes and increasingly strict regulations regarding sulfur content of fuels, better hydrotreating catalysts are sought. This requires a deeper understanding of the structure and function of transition metal sulfide-based catalysts used in refineries. Indeed, alumina-supported molybdenum-based hydrotreating catalysts promoted by cobalt or nickel are industrial "workhorses" for upgrading petroleum-based fuels. Basic functions that describe catalyst activity such as the role of promoters (Co, Ni) and the role of carbon are becoming better understood [1]. There has been much progress in the elucidation of the nature of

* Corresponding author. Fax: (+1)915-747-6007.
E-mail address: myrperez@utep.edu (M.P. De la Rosa).
[1] Present address: Institut de Recherches sur la Catalyse, CNRS, 2 avenue Albert Einstein, 69626 Villeurbanne cedex, France.

0021-9517/$ – see front matter
doi:10.1016/j.jcat.2004.03.039

the synergetic effect of Co (or Ni). Many structural models have addressed the cobalt-promotion effect [2–5]. However, the first direct observation of a distinct Co environment was obtained by Wivel et al. [5] using Mössbauer spectroscopy: cobalt atoms were located at the edges of MoS_2 layers forming the so-called "Co–Mo–S" phase. Recently, using scanning tunneling microscopy (STM), Lauritsen et al. [6] observed that cobalt atoms were found to prefer locations at the so-called sulfur-terminated edges resulting in truncated hexagonal structures. Apart from these advances in the structural characterization of Co–Mo nanostructures, theoretical calculations using density-functional theory (DFT) have led to considerable progress in explaining the electronic origin for promotion [7–9]. Finally, although the role of carbon in transition metal sulfide catalytic materials has been largely ignored due to the difficulty of characterizing carbon on catalysts stabilized under the conditions of hydrotreatment, recent studies have emphasized that carbon plays an important role in hydrotreating reactions. Two main effects were observed: (1) a geometrical effect by which carbon deposit enhances dispersion [10,11] stabilizing small MoS_2-like particles and (2) a structural effect by which surface carbide-like species are formed at the surface of the active phase during the HDS reaction [12–15].

MoS_2 presents a layered sandwich S–Mo–S structure with Mo at the center of a trigonal prism formed by six sulfur atoms. The MoS_2 layers are weakly bonded to each other by van der Waals forces leading to a highly anisotropic stacked configuration in the [001] direction [16]. Chemical properties vary according to the planes exposed to the reactants. While the basal planes with completely coordinated sulfur atoms are thought to be inert, edge planes are known to be highly reactive [17,18]. The ratio between the edge plane/basal plane, i.e., the slab length, is therefore of primary importance in obtaining highly active MoS_2-based catalysts. Morphology of the MoS_2 particles also plays an important role with regard to changes in selectivity. It is generally admitted that two different active sites exist on MoS_2-based catalysts as developed by Daage and Chianelli in the rim-edge model [19]. For nonpromoted Mo systems, the two different sites are differentiated according to their location on the edge. One site called the "rim" site is located at the edge of exterior layers and is active for both hydrogenation and desulfurization reactions while sites on interior layers called "edge" sites are active only for direct desulfurization. The proportion of rim sites and selectivity is independent of the particle diameter and varies only with the stacking height. This model shows that to determine precisely the catalyst dispersion is fundamental in establishing a structure/function relationship.

Progress in completely understanding the nature of the active phase has been hampered by the difficulty in determining catalyst dispersion correctly. Indeed, molybdenum disulfide presents a very disordered and poorly crystalline state in real hydrotreating conditions (the "rag" structure) [20]. Support interaction with the active phase is an additional confusing parameter. Many characterization techniques, particularly X-ray absorption fine structure (XAFS), X-ray diffraction (XRD), and high-resolution electron microscopy (HREM) have been used extensively to study HDS catalysts. However, all these techniques have limitations in determining the dispersion of the active phase. XAFS suffer from the intrinsic structural disorder at the periphery of the slabs [21–25] and from bending curvatures of the MoS_2 basal plane [26]. Consequently, underestimation of the Mo–Mo coordination number and therefore of the particle size of the slabs was generally observed. Moreover, no information about stacking can be obtained using XAFS.

Even if successful in addressing many crucial problems in HDS, electron microscopy has failed to give a clear picture of the CoMoS phase on alumina because of interference from the support in commercial catalysts. Visualization of slabs depends on the support used and on the type of exposed planes leading to bonding of the layers either by the basal plane or by the edge planes. Basal-bonded layers could not be visualized particularly if thick substrates are used while edge-bonded layers are visible [27]. However, even in that case, a tilt of 5° from the normal direction to the support is sufficient to make particles undetectable [28]. HRTEM is "seeing" less than 10% of the active phase. Nevertheless, HRTEM remains a valuable technique to get an overview of the catalyst dispersion in order to address ambiguities.

XRD line profile analysis may be used but the asymmetry broadening of the mixed (100) + (101) peaks makes the determination of the dispersion along the basal direction difficult (see Fig. 1). The asymmetry of the (100) envelope is characteristic of layer lattice structures in which the layers are displaced randomly with respect to one another like a spread deck of cards [29]. As demonstrated by Liang et al., imperfect stacking and bending effects results only in a small

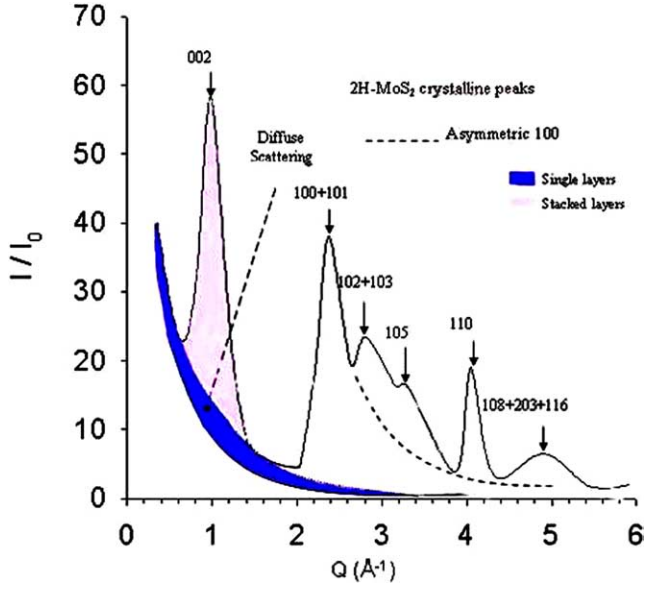

Fig. 1. Typical X-ray diffraction profile of the poorly crystalline MoS_2 phase. The positions of the main diffraction peaks are indicated by arrows.

displacement of the position of the (002) and (110) reflections without peak broadening (see Fig. 1) while the (100) envelope can be strongly modified by stacking faults [30]. Therefore, stacking along the [001] direction can be determined for unsupported catalysts using the Debye–Scherrer equation applied to the (002) diffraction peak. However, in the case of real commercial-supported catalysts, all MoS_2 characteristic XRD peaks vanished leading only to broad signals due to the support. Moreover, it is quite important to note that the determination of the stacking degree using the Debye–Scherrer equation for the (002) peak gives an average value for stacked layers only. Indeed, the Debye–Scherrer equation ignores the single slabs, since it only applies to the (002) diffraction peak. This leads to very approximate results using this equation particularly at small stacking values generally observed for well-dispersed commercial MoS_2-based catalysts. A full scattering model is then required to evaluate the fraction of unstacked layers giving rise to an excess diffuse scattering under the (002) peak (see Fig. 1) and of stacked layers determined by the (002) peak [20]. Indeed, X-ray scattering using synchrotron radiation is well suited to study MoS_2-based catalysts that yield diffuse scattering patterns attributed to stacking and rotational disorder of the layers. This technique provides a clear picture of unstacked or stacked MoS_2 layers in supported HDS CoMo catalysts and removes any ambiguity about the determination of the dispersion. The synchrotron source increases substantially the signal to noise ratio and can reveal specific features otherwise ambiguous or undetectable using classical sources of X-rays.

The aim of the present study was to benefit from a full description of the morphology of supported MoS_2-based catalysts to determine the influence of different parameters affecting their dispersion: support interaction (SiO_2, Al_2O_3), effect of the hydrodesulfurization of dibenzothiophene (DBT), and aging of commercial catalysts in industrial hydrotreating conditions. We investigated the structural active phases of commercial and model catalysts by X-ray-scattering measurements at the Stanford Synchrotron Radiation Laboratory (SSRL). A qualitative analysis of the commercial $CoMo/Al_2O_3$ catalyst was performed using HRTEM in order to compare the two techniques. This study is part of a general effort to better describe structure/function relationship in hydrotreating catalysts.

2. Experimental

2.1. Catalyst preparation and properties

Five different supported CoMo catalysts were used to perform this study. Three are commercial $Co/MoS_2/Al_2O_3$ catalysts (IMP-DSD14) that differ by their time of use, the first runs for 1 week and the second runs for 1 month in a pilot plant, and the third runs in an industrial plant for 4 years. The catalyst was removed from the industrial reactor after 4 years in a regularly schedule turn around and was still active as confirmed by model compound reaction studies. The characteristics of the commercial catalyst used to perform hydrotreating reactions in pilot and industrial plants are listed in Table 1. The run conditions for the two pilot plant experiments were: LHSV $= 2.5\ h^{-1}$, $P = 5.5$ MPa, $T = 350$–$370\,^{\circ}C$ under virgin gas oil. These catalysts were run under these conditions for 1 week and 1 month, respectively. The run conditions for the industrial plant were: LHSV $= 1.5\ h^{-1}$, $P = 7.8$ MPa, $T = 340$–$360\,^{\circ}C$. The characteristics of the feedstock of the pilot plant that represent similar conditions to those in the industrial plant are presented in Table 2. The third catalyst was run in an industrial plant for 4 years and it treated 25,000 barrels/day (20,000 barrels gas oil (similar to pilot plant gas oil) mixed with 5000 barrels of light cycle oil). The commercial catalysts run for 1 week, 1 month, and 4 years are labeled respectively D-1W, D-1M, and D-4Y.

Table 1
Characteristics of the commercial $CoMo/Al_2O_3$ catalyst

$CoMo/Al_2O_3$ (DSD14)	
Shape	Trilobular
Size	1/10 inch
Surface area	227 m^2/g
Pore volume	0.49 cm^3/g
Pore diameter avg.	59 Å
Compact density	0.73 g/cm^3
Crush strength	3.2 kg/mm
Mo (wt%)	12.5
Co (wt%)	3.0
P (wt%)	1.4

Table 2
Properties of the feedstock used in the pilot plant

Feedstock	SRGO[a] Tula 0501
Sulfur (wt%)	1.61
Total aromatic (wt%)	35.5
Total nitrogen (ppmw)	502
Basic nitrogen (ppmw)	152
Specific weight	0.8702
Distillation ASTM-D-86	
IBP (°C)	224
5/10 vol% (°C)	269/283
30/50 vol% (°C)	304/317
70/90 vol% (°C)	329/347
FBP (°C)	362

[a] Straight Run Gas Oil.

These solids were also compared to model catalysts prepared using alumina and silica supports presenting similar surface areas and pore volumes. The γ-Al_2O_3 support has a surface area of 240 m^2/g and a pore volume of 0.56 cm^3/g. The silica support (Degussa Aerosil D200) has a surface area of 200 m^2/g and a pore volume of 0.47 cm^3/g. The model $CoMo/Al_2O_3$ and $CoMo/SiO_2$ catalysts were prepared by incipient wetness impregnation of the different supports with an aqueous solution of ammo-

nium heptamolybdate, $(NH_4)_6Mo_7O_{24} \cdot 4H_2O$ (Fluka). The Mo-impregnated support was then mixed with an aqueous solution of cobalt nitrate, $Co(NO_3)_2 \cdot 6H_2O$ (Fluka). The catalysts were dried at 120 °C and calcined under air flow at 500 °C. The $CoMo/Al_2O_3$ catalyst contained 15.2 wt% MoO_3 and 4.3 wt% CoO. The $CoMo/SiO_2$ catalyst contained 14.8 wt% MoO_3 and 5.7 wt% CoO.

Sulfidation for the model catalysts was carried out in a microflow reactor at 400 °C—10 h at atmospheric pressure under a 10% H_2S/H_2 (v/v) sulfiding mixture. After this activation procedure, the solids were cooled to room temperature in the presence of the sulfur-containing atmosphere, flushed with an oxygen-free nitrogen flow, and stored in Schlenk tubes under argon. The industrial catalysts were not presulfided; sulfidation was performed from the sulfur present in the feedstock and under the conditions of the different reactors used.

2.2. HDS reaction conditions

The hydrodesulfurization of dibenzothiophene was used to evaluate morphological changes of the model catalysts when submitted to the experimental conditions of hydrotreatment (high H_2 pressure, presence of a hydrocarbon solvent). The reaction was carried out in a flow reactor at 290 °C under 4.0 MPa total pressure. The reactant mixture consisted of dibenzothiophene (1.11 mol%) diluted in decalin. Dibenzothiophene (98%) and decalin (98%) were purchased respectively from Aldrich and Fluka. To avoid diffusion limitations, catalysts (100 to 300 mg) were diluted with SiC before being placed in the tubular reactor. The reactant mixture was injected by a high-pressure liquid pump. The various partial pressures were $P_{H_2} = 3.06$ MPa, $P_{DBT} = 0.01$ MPa, and $P_{decalin} = 0.93$ MPa. The H_2/HC ratio was kept constant at 470 l/l. Contact time was adjusted during the HDS run in order to get similar total conversions. Catalyst activity was determined according to the following equation considering a pseudo-first order for the individual HDS rate constant,

$$k = \frac{F}{m} \ln\left(\frac{1}{1-\tau}\right),$$

where F is the molar feed rate of reactant in mol s^{-1}, m is the catalyst weight in grams, and τ is the total conversion of DBT.

2.3. HF treatment

Spent $CoMo/Al_2O_3$ catalyst, freshly sulfided $CoMo/Al_2O_3$, and $CoMo/SiO_2$ model catalysts were etched with hydrofluoric acid to remove the support. The acid treatment consisted of placing 1 g of catalyst in 50 ml of 47% HF for 8 h [31]. After the treatment the catalyst was filtered out and washed with water several times until no oily residue was present.

2.4. X-ray data collection

The X-ray-scattering data were collected at SSRL (Stanford Synchrotron Radiation Laboratory) on beamline 2-1. To maintain the parallel beam geometry of the diffractometer, and to reduce the background from other scattering sources, a 1 mrad soller slit was used in the vertical collimating geometry before a NaI photomultiplier tube. The size of the focused beam was 2×1 mm and approximately 10^{11} photons/s were incident on the sample. The XRD patterns were collected in the 0.3–6 Q range at 7.0 keV ($\lambda = 1.7712$ Å).

Quantitative information could be obtained using the X-ray-scattering intensity for a collection of atoms,

$$I_{eu} = \sum_m \sum_n f_m f_n e^{iQ \cdot R_{mn}},$$

where f_m is the X-ray atomic-scattering factor of m-type atoms, $\mathbf{Q}$ is the X-ray-scattering wave vector with $Q = |Q| = 4\pi \sin\theta/\lambda$, and the vector $\mathbf{R}_{mn}$ connects atom m and atom n. Assuming a random (powder) arrangement of the structure with respect to the incoming X-ray beam, a spherical average gives the Debye-scattering equation:

$$I_{eu} = \sum_m \sum_n f_m f_n \frac{\sin QR_{mn}}{QR_{mn}}.$$

The full widths at half-maximum (FWHM) of the (002) peaks were measured directly from the X-ray patterns in order to approximate crystallite dimensions of the MoS_2 slabs in the c axis direction using the Debye–Scherrer relation,

$$D_{002} = \frac{k_{002}\lambda}{\beta_{002}\cos\theta},$$

where D_{002} is the dimension of the particle along the stacking direction, λ is the wavelength of the X-rays ($\lambda = 1.7712$ Å), θ is the diffraction angle, and β_{002} (or FWHM) is the angular line width. The shape factor k_{002} depends on the shape of the particle and is equal to 0.76 for MoS_2 [19,30]. The apparent average number of layers was calculated using $\bar{n} = D_{002}/6.17$ (D_{002} in Å), the value of 6.17 Å corresponding to the interlayer spacing in the 2H-MoS_2 structure. The crystalline order along the basal direction can be evaluated using the Debye–Scherrer equation applied to the broadening of the (110) diffraction peak. As for the (002) peak, the (110) peak is not influenced by imperfect stacking or bending/folding of the layers. In that case, the shape factor k_{110} varies with the β_{110} angular linewidth but it can be determined following the values reported by Liang et al. [30] using computer calculations of the scattered X-ray intensity for model MoS_2 structures. According to the experimental angular line widths measured in the present study, k_{110} values vary between 1.42 and 1.56.

The (002) broadening of the diffraction peak can be calculated directly from the X-ray patterns of the different supported catalysts. However, the strong (333) Al_2O_3 peak partly masks the (110) MoS_2 diffraction peak at $Q = 4$ Å^{-1}.

Therefore, for high values of Q, X-ray patterns were normalized to the (440) Al_2O_3 peak before subtraction. The resulting patterns after subtraction resemble those found for the poorly crystalline unsupported MoS_2 phase. For silica-supported catalysts, no SiO_2 reflections interfere with the (110) MoS_2 peak and direct measurements of the FWHM value can be performed.

The line broadening analysis was complemented by a full scattering model. The full scattering model evaluates the area of the 002 peak and the diffuse scattering area under the 002 peak to determine the fractions of stacked and unstacked layers. In order to integrate the total area, the low angle data was normalized to the (111) Al_2O_3 peak prior to subtraction. Alumina reflections were then removed from the total scattering by a point-by-point subtraction of scaled support XRD patterns using the tables and graphs modules from Cerius^2 3.4 (Accelrys Inc.). The resulting areas of the (002) peak and the diffuse area under the peak correspond to the respective contributions of stacked and unstacked layers of the commercial catalysts. The relative proportions of stacked and unstacked layers were then directly obtained from the XRD data (see Fig. 1).

2.5. Transmission electron microscopy

High-resolution electron microscopy studies were performed in a Jeol 2010F electron microscope operating at 200 kV. The microscope is equipped with a Schottky-type field emission gun and an ultrahigh resolution pole piece ($C_s = 0.5$ mm; point resolution, 1.9 Å). The field emission gun provides a highly coherent intense beam (intensity $\sim 10^5$ electrons/(nm^2 s)). The specimens for TEM analysis were pulverized and suspended in isopropanol at room temperature and ultrasonically dispersed. A droplet of the suspension was placed on a holey carbon film supported on a copper grid (200 mesh). The elemental composition was determined by energy dispersive X-ray (EDX) spectroscopy with an Oxford INCA spectrometer fitted to the TEM, using a spot size of 1.0 to 0.5 nm. Images of the prepared samples were obtained at the Scherzer defocus. This condition depends on the accelerating voltage of the microscope and the spherical aberration of the lenses in the microscope and it can be calculated from the following equation,

$$\mathrm{Sch} = -\sqrt{C_s \lambda_e},$$

where C_s is the spherical aberration and λ_e is the wavelength of the electrons at the particular accelerating voltage.

3. Results

3.1. HF treatment of supported CoMo catalysts

In supported catalysts, the principal role of the support is to disperse the active phase and to prevent it from sintering under catalytic conditions. In addition to these physical interactions, catalyst supports often affect the catalytic properties of the supported metals through electronic or structural interactions [32,33]. Using classical X-ray studies to obtain information about the structural change of the metal/support interface is often difficult because the scattering contributions from the metal particles and from the support partially overlap leading to the complete disappearance of any characteristic features of the active phase if well dispersed on the support. The support contribution was suppressed in order to acquire information of the morphology of the active phase. Treatment with hydrofluoric acid of freshly sulfided $CoMo/Al_2O_3$ catalyst was used to remove the support using the method reported previously by Pollack et al. [31].

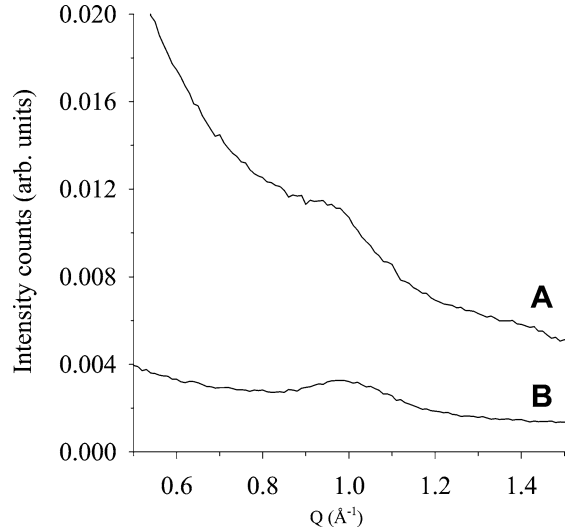

Fig. 2. Low-angle X-ray synchrotron patterns for the freshly sulfided model $CoMo/Al_2O_3$ catalyst before (A) and after (B) the HF treatment.

The low-angle X-ray patterns of freshly sulfided model $CoMo/Al_2O_3$ catalyst before and after HF treatment are shown in Fig. 2. The (002) peak at about $Q = 1.0$ Å^{-1} is significantly broad in both cases. Clearly, the catalyst underwent a substantial reorganization after the removal of the support. Indeed, the remaining acid used to treat the catalyst turned pink from clear, suggesting that cobalt metal was extracted from the catalyst. Energy Dispersive X-ray analysis of the catalysts before and after the HF treatment confirmed a nonnegligible loss of cobalt content (50% for $CoMo/Al_2O_3$ and 38% for $CoMo/SiO_2$). The etching process of CoMo catalysts by HF seems to disturb part of the CoMoS phase. Analysis of the stacking dimensions along the c direction showed a "destacking" process. For $CoMo/SiO_2$, the average stacking decreases from $\bar{n} = 6.1$ to $\bar{n} = 4.2$ while a smaller yet significant decrease from $\bar{n} = 4.7$ to $\bar{n} = 4.2$ is found for $CoMo/Al_2O_3$.

The apparent increase of the intensity of the (002) peak after the HF treatment while the peaks become broader is due to the removal of the support by the HF treatment leading to the suppression of the scattering contribution coming from the support. Determination of the crystalline order along the basal direction reveals a different comportment

when compared to the stacking height evolution. Only a negligible decrease of the D_{110} values was observed after the etching process since lateral dimensions hardly changed from $D_{110} = 64$ Å to $D_{110} = 60$ Å for $CoMo/SiO_2$ and from $D_{110} = 44$ Å to $D_{110} = 38$ Å for $CoMo/Al_2O_3$. The HF treatment results in a modification of the degree of dispersion for both alumina- and silica-supported catalysts and is therefore not an appropriate technique.

3.2. Effect of the dibenzothiophene hydrodesulfurization test on the stacking of CoMo catalysts

The inherent difficulty of determining structural, morphological, and textural changes of hydrodesulfurization catalysts during reaction has limited our understanding of the real nature of the active phase in steady-state catalytic conditions particularly if high pressure and high amounts of H_2S or hydrocarbons are present during the process. However, the structure and morphology of a heterogeneous catalyst are extremely dependent on reaction conditions and any process may impose a possible modification of the active phase during hydrodesulfurization [34]. Indeed, carbon uptake during hydrotreating conditions generates structural changes of the MoS_2 active phase. Previous studies by Chianelli and co-workers have reported that surface carburization of (Co)/MoS_2 catalysts occurs during the HDS run; carbon atoms replace sulfur atoms at the edges of MoS_2 layers forming surface carbide-like entities [12,13].

Hydrodesulfurization of dibenzothiophene is nowadays the standard catalytic test to evaluate activity of catalysts under hydrotreating conditions. Therefore, the effect on dispersion of this catalytic test was determined for supported CoMo catalysts. The low-angle X-ray patterns of the freshly sulfided $CoMo/Al_2O_3$ and DBT-tested $CoMo/Al_2O_3$ catalysts are illustrated in Fig. 3. The (002) peak is visible prominently in the fresh catalyst sulfided at 400 °C under atmospheric pressure while the stacking gives rise only to a slight rise between 0.8 and 1.2 $Å^{-1}$ when DBT conditions are applied. The decrease in intensity of the (002) peak implies a decrease in stacking of the MoS_2 slabs under reactor conditions. This effect was also clearly observed on $CoMo/SiO_2$. Average stacking numbers and HDS activities are listed in Table 3. Even if an evident decrease in stacking is observed, differences could be ascertained between alumina and silica-supported catalysts. While the decrease in stacking is quite noticeable for $CoMo/Al_2O_3$ with almost only single layers when the catalyst is submitted to HDS conditions, the effect is less pronounced for $CoMo/SiO_2$ with only 25% decrease in stacking. Table 3 also suggests that even if single-layered entities are uniquely formed on $CoMo/Al_2O_3$, its activity is 60% higher than on $CoMo/SiO_2$. These results show that the DBT HDS test alone modifies the morphology of the MoS_2-based catalysts, decreasing the stacking of the active phase.

Consequently, based only on average stacking values calculated using the Scherrer equation applied to the (002) peak, a high proportion of multistacked entities is expected on the silica-supported catalyst while only single-layered CoMo species exist on the alumina-supported catalyst [35]. However, such an assumption will lead to an erroneous overview of the real dispersion of the active phase for these supported HDS catalysts. Indeed, as noted before, average stacking values based on the Scherrer equation completely ignore single-layered particles. A full scattering model was then used to determine the proportion of single slabs giving rise to excess scattering underneath the (002) peak. Such a model showed that the proportion of unstacked layers is still very high. Indeed, after HDS conditions were applied, $CoMo/Al_2O_3$ exhibited almost only unstacked layers (98%) while the proportion of stacked layers is only 7% for the $CoMo/SiO_2$ catalyst. Then, in any case, stacking variations for these catalysts correspond only to a minor amount of the layers. However, it should be kept in mind that expected variations of selectivity would still depend on these stacked particles [19].

Compared to the stacking decrease under HDS conditions, crystalline order lengths along the [110] direction show a different evolution. Both $CoMo/Al_2O_3$ and

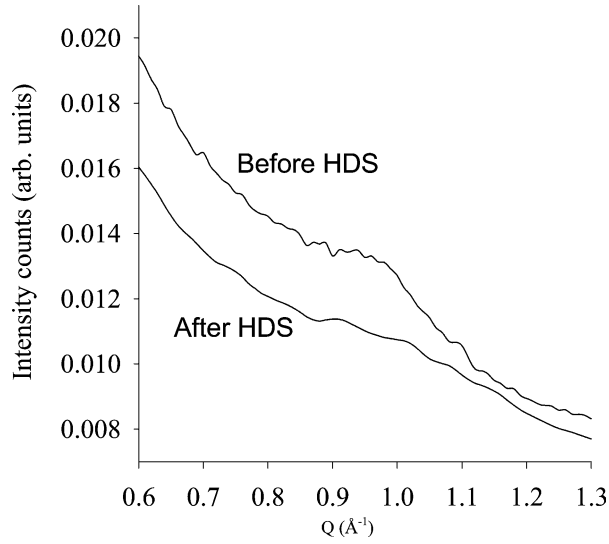

Fig. 3. Effect of the HDS conditions on the evolution of the (002) signal at $Q = 1.0$ $Å^{-1}$ for the model $CoMo/Al_2O_3$ catalyst.

Table 3
Average stacking numbers, ratio stacked/unstacked particles, crystalline order lengths along the basal direction, and HDS activities for model $CoMo/Al_2O_3$ and $CoMo/SiO_2$ catalysts before and after the HDS test

		$CoMo/Al_2O_3$	$CoMo/SiO_2$
$\bar{n}$	Before HDS	4.7	6.1
	After HDS	1.0	4.0
Ratio stacked/ unstacked	Before HDS	5/95	12/88
	After HDS	2/98	7/93
D_{110} (Å)	Before HDS	44	64
	After HDS	46	66
HDS activity (10^{-7} mol g^{-1} s^{-1})		8.1	5.0

$CoMo/SiO_2$ catalysts do not present any real growth of lateral dimensions when the HDS test was applied since D_{110} values remain constant at ~ 45 Å for $CoMo/Al_2O_3$ and at ~ 65 Å for $CoMo/SiO_2$ (Table 3). Consequently, HDS conditions involve a "destacking" phenomenon on both types of supported catalysts whereas lateral dimensions are not really modified. The main cause for the change in dispersion during the HDS test is the stacking height decrease. The HDS test leads to a redispersion of CoMo particles which is accentuated when a strong interacting support like alumina is present. This higher dispersion of the $CoMo/Al_2O_3$ catalyst has consequences on the HDS activity. Indeed, as shown in Table 3, the better dispersed $CoMo/Al_2O_3$ catalyst presents a 60% higher HDS activity than $CoMo/SiO_2$.

3.3. *Effect of industrial processing conditions on the morphology of commercial catalysts*

Particle-size determination of cobalt-promoted and supported MoS_2 catalysts is crucial to understand the activity and selectivity of this class of catalysts since it provides information about the number of active sites available. MoS_2 crystallite dimensions of commercial catalyst operating in real industrial hydrotreating conditions were determined by X-ray line-broadening analysis. The same commercial $CoMo/Al_2O_3$ catalyst has been studied at three different stages of its catalytic life: 1 week (D-1W) and 1 month (D-1M) in a pilot plant at 5.5 MPa for the HDS of a straight run gas oil (SRGO) and four years (D-4Y) in a commercial unit working at 7.8 MPa for the HDS of a blend of SRGO (80 vol%) and light cycle oil (LCO) (20 vol%). A qualitative analysis of the commercial $CoMo/Al_2O_3$ catalyst was also performed using HRTEM for the D-1M and the D-4Y samples in order to evaluate the two techniques. The wide-angle X-ray patterns of the commercial catalyst at its three different stages of its catalytic life are illustrated in Fig. 4. The alumina X-ray pattern is also shown for comparison. The (100) and (110) peaks from MoS_2 partly overlap with the (220) and (333) peaks from the support. All commercial catalysts present low stacking as observed from the (002) peak at $Q = 1.0$ Å^{-1}. The low angle X-ray-scattering intensities (Fig. 5) of the three samples of the commercial catalyst reveal a progressive disappearance of the broad (002) signal with time of use. Moreover, the strong diffuse scattering present at low angles is mainly due to uncorrelated single layers [29]. While the D-1W sample still shows a discernable (002) peak, the D-1M sample presents a decreasing signal which disappears completely on the D-4Y sample. Then, after being in the reactor for 1 week, determination of the scattering for unstacked and stacked layers shows that the catalyst still presents 6% of stacked layers; after 1 month the proportion decreases to 3% of stacked layers, and after 4 years of usage it shows almost no stacking. Finally, careful analysis of the (100) peak reveals an evolution of its intensity with time of use showing a progressive change of stacking faults particularly between the D-1W and the D-1M samples

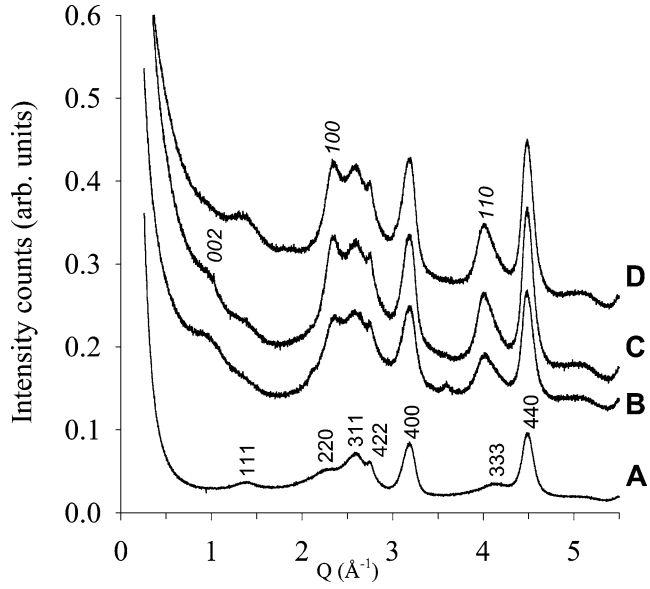

Fig. 4. Wide-angle X-ray-scattering intensities for the alumina support (A) and the commercial $CoMo/Al_2O_3$ catalyst at the three different stages of its catalytic life: 1 week (B), one month (C), and 4 years (D). The main alumina and MoS_2 diffraction peaks are shown on the X-ray patterns; peaks for the MoS_2 phase are shown in italics.

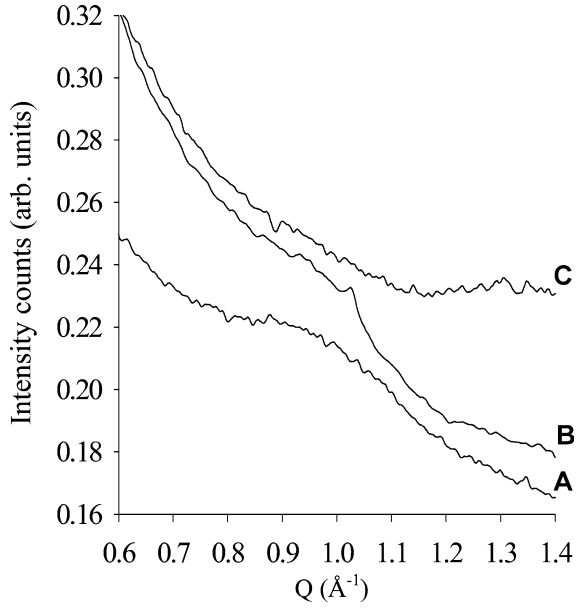

Fig. 5. Low-angle X-ray synchrotron patterns for the commercial $CoMo/Al_2O_3$ catalyst at the three different stages of its catalytic life: 1 week (A), 1 month (B), and 4 years (C).

without influencing the (002) and (110) peaks, as expected from the previous study by Liang et al. [30].

The crystalline order lengths for the three samples changed from 52 Å for the D-1W sample to 63 Å for the D-4Y catalyst showing a lateral growth. The results suggest that lateral growth is a slower process compared to "destacking." The increase in lateral dimensions results in a decrease in activity between D-1W and D-4Y since larger lateral di-

mensions correspond to a lower proportion of Mo edge sites compared to the total number of Mo atoms per crystallite.

The higher signal to noise ratio of the synchrotron source also revealed the presence of weak signal at about $Q = 2.0$ Å^{-1} and $Q = 3.6$ Å^{-1} corresponding to the (311) and (440) diffraction peaks of the Co_9S_8 phase. During steady-state working conditions in an HDS pilot plant the Co_9S_8 peaks diminished in intensity from 26 to 9% in the D-1W and D-1M samples, respectively. The D-4Y sample shows only 4% in intensity and a shoulder at $Q = 3.0$ Å^{-1} corresponding to the (002) signal of the Co metallic phase, as shown in Fig. 6. Moreover, distinctive Co nanoparticles were observed on the D-4Y catalyst (cf. Fig. 7). Fourier-transformed picture and filtered image of a cobalt particle and Fast Fourier transform showing the interplanar distances corresponding to the formation of cobalt nanoparticles (see inset). Therefore, X-ray synchrotron analysis confirms the presence of an initial Co_9S_8 phase in low proportion, which tends to be reduced into Co^0 metallic nanoparticles when severe conditions are applied.

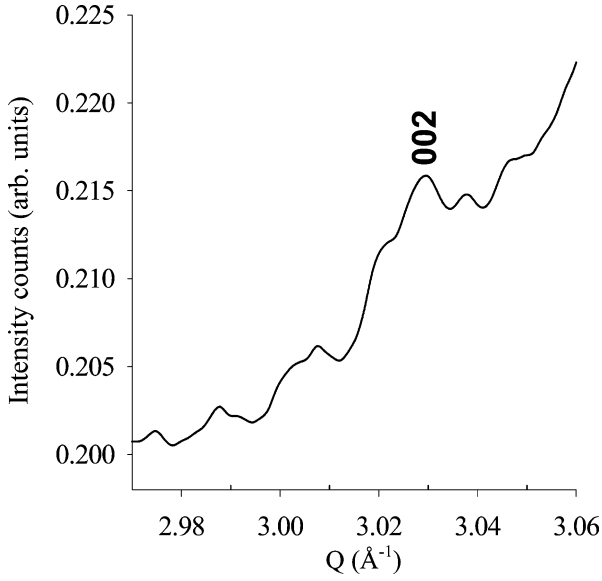

Fig. 6. The (002) signal of the Co metallic phase found in the D-4Y commercial $CoMo/Al_2O_3$ catalyst.

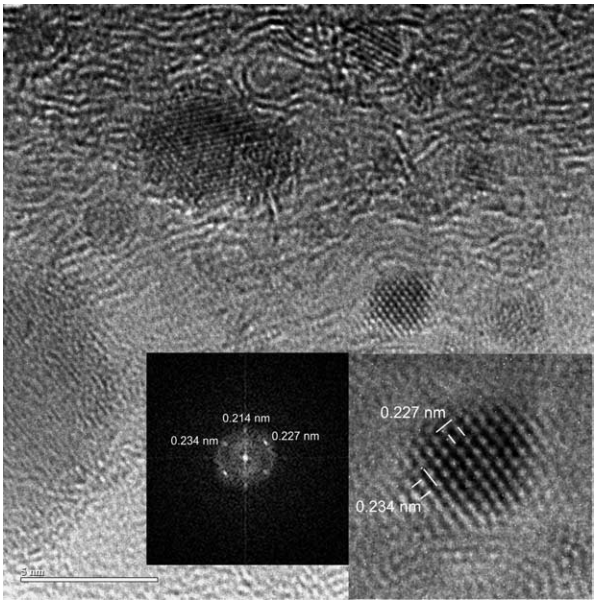

Fig. 7. HREM micrograph of the D-4Y commercial $CoMo/Al_2O_3$ catalyst showing the presence of Co nanoparticles. Insets: Fourier-transformed picture and filtered image of one of the Co particles.

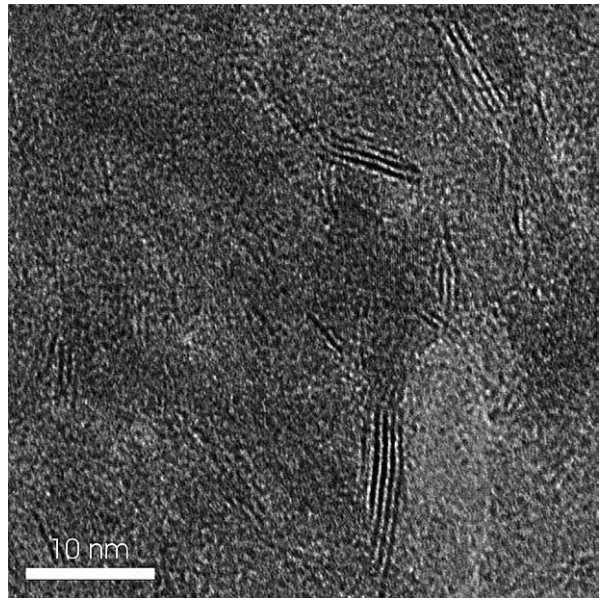

Fig. 8. TEM micrograph of the commercial $CoMo/Al_2O_3$ catalyst after 1 month in a HDS pilot plant.

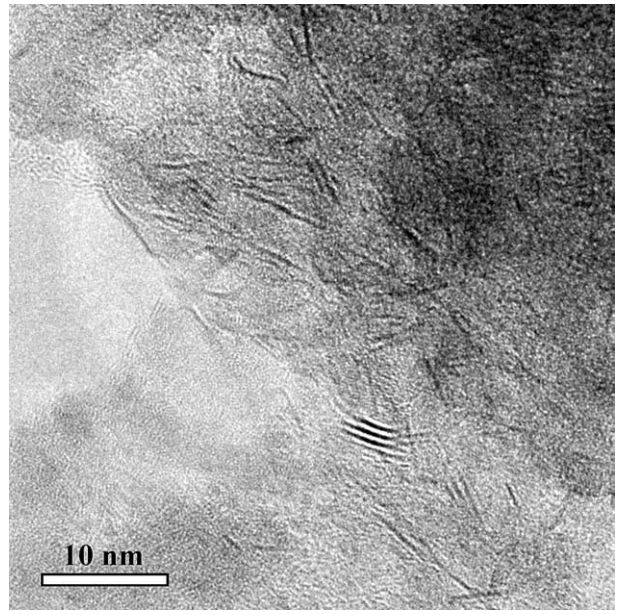

Fig. 9. TEM micrograph of the commercial $CoMo/Al_2O_3$ catalyst after 4 years in a HDS industrial unit.

A qualitative analysis of the commercial $CoMo/Al_2O_3$ catalyst was performed on the D-1M and the D-4Y samples using HRTEM. Micrographs of the D-1M and D-4Y samples are reported Figs. 8 and 9, respectively. The images of the samples were obtained using the closest to Scherzer defocus. Experimental HREM images of D-1M revealed typical MoS_2 layered fringes of about 0.6 nm, which is close to the (002) plane spacing of 0.615 nm corresponding to the S–Mo–S layers, visualized as parallel dark lines observed in Fig. 8. A high proportion of stacked layers consisting of 2 to 4 layers is still clearly visible on the D-1M sample. Comparison with the HRTEM micrograph of the D-4Y sample shows an increase in the number of particles consisting of only one or two stacked layers. Therefore, HRTEM analysis qualitatively confirms a decrease in stacking between the two samples. Unfortunately not all of the active phase is adequately oriented or thin enough to be visible in the microscope. Under these conditions, 90% of the active phase is missed by the microscope. Statistics performed on nine different pictures gave an average slab length and a mean value for the stacking number reported in Table 4. Comparisons between D_{110} values calculated on X-ray patterns and slab lengths determined on TEM pictures are in relatively good agreement even if TEM seems to slightly overestimate these lengths. However, when compared to the average stacking values measured by X-ray synchrotron analysis, more stacked layers seem to be detected by HRTEM. The dependence on the orientation of the crystal and the local nature of this technique has to be accounted for when analyzing HRTEM data. A high percentage of single slabs was therefore clearly underestimated using only HRTEM. This fact is even accentuated if HRTEM data are compared to the ratio unstacked/stacked layers which shows that more than 90% of the particles are formed with single layers. A full scattering evaluation is then quite necessary in order to evaluate precisely the morphology of MoS_2 particles.

Table 4
Average stacking numbers (XRD, HRTEM), crystalline order lengths along the (110) direction (XRD), ratio stacked/unstacked particles, slab length (HRTEM) and HDS activity for the commercial $CoMo/Al_2O_3$ catalyst at its three different stages of catalytic life

$CoMo/Al_2O_3$ (DSD-14)		D-1W	D-1M	D-4Y
XRD	$\bar{n}$	1.7	1.5	1.0
	D_{110} (Å)	52	57	63
	Ratio stacked/unstacked	6/94	3/97	0/100
HRTEM	$\bar{n}$	/	4.0	2.5
	L (Å)	/	65	72
	$\Delta\bar{n}$	/	±2.5	±1.5
	Δslab length	/	±8	±9
HDS activity (10^{-7} mol s^{-1} g^{-1})		14.5	12.4	11.1

Comparison was made between HRTEM and XRD about stacking numbers and slab lengths (assuming that gives the real slab length value).

4. Discussion

The high anisotropic nature of the MoS_2 active phase of hydrotreating catalysts represents a challenge when characterizing this type of catalytic system. Activity varies with the proportion of edge and basal planes exposed to the reactants. While edge planes presenting coordinative unsaturated sites (CUS) are known to be active for HDS reactions, basal planes are considered to be nearly inert due to the complete coordination of its sulfur atoms [17,29]. The bidimensional nature of the MoS_2 structure can also lead to the formation of stacked slabs maintained altogether only by Van der Waals forces. Determination of the particle size along the basal and the stacking direction is therefore fundamental in order to determine the real degree of dispersion. However, the inherent disordered structure of the MoS_2 phase particularly at the periphery of the slabs makes the determination of the dimensions of the particles quite problematic using XAFS, TEM, or classical X-ray diffraction particularly for supported catalysts. Therefore, a full scattering model should be used for well-dispersed supported catalysts. The use of a synchrotron source increasing the signal to noise ratio makes the determination of diffraction signals otherwise undetectable by classical X-ray possible. Stacking evolution can then be followed for supported catalysts using synchrotron X-ray scattering and can give a clear picture of the morphology of HDS catalysts in relation with different parameters influencing dispersion: type of support, effect of the HDS test, and/or ageing in industrial processing conditions.

The first part of our study was to determine if the removal of the support by a HF treatment could be a valuable solution to evaluate the dispersion of MoS_2-based catalysts. However, the dissolution of the support by a hydrofluoric acid solution led to a partial destruction of the active phase with loss of cobalt and reorganization of the MoS_2 particles into less stacked slabs. The effect of hydrotreating operating conditions should also be considered since the catalyst active structure is known to be dynamic and could be modified by reactants or varying operational conditions. Nevertheless, studies addressing the effect of HDS conditions on the morphology of MoS_2 slabs have been exclusively obtained using TEM [31,36–40]. The results related to MoS_2 slabs degree of stacking under operating conditions are very inconclusive and vary from an increase [36,37,40] to an absence of variation [39] or even to a decrease of the stacking under operating conditions [31,38]. Similarly, results are contradictory when considering slab length along the basal direction. Eijsbouts and co-workers [36,37] have reported that a $NiMo/Al_2O_3$ catalyst used 1 week in a pilot plant for the hydrodenitrogenation (HDN) of a vacuum gas oil (VGO) feedstock at 10.0 MPa and 390 °C presents an increase of both stacking and dimension along the basal direction. Ni et al. [40] have obtained similar results for a phosphorus-doped $NiMo/Al_2O_3$ catalyst used in a HDN unit 1.5 years at a hydrogen pressure of 17.0 MPa and 390 °C. Yokoyama et al. [39] claimed that an increase in lateral dimensions but no in-

crease in stacking was observed for a $CoMo/Al_2O_3$ catalyst used 1 year in a commercial HDS unit for upgrading VGO at 5.9 MPa and 360–400 °C. Contrary to these results, Pollack et al. [31] found a destacking process on a $NiMo/Al_2O_3$ catalyst used for upgrading coal liquids. Finally, Weissman et al. [38] observed a destacking effect but a lateral growth for a $CoMo/Al_2O_3$ catalyst used 255 h for upgrading LCO at 3.4 MPa and 400 °C. All these studies showed that electron microscopy studies should be used cautiously to ascertain changes in morphology.

X-ray synchrotron analysis of a model $CoMo/Al_2O_3$ or $CoMo/SiO_2$ catalyst before and after a standard catalytic HDS test demonstrates a destacking phenomenon when HDS conditions are applied under steady-state conditions. A similar effect was observed with commercial CoMo catalysts operating in real industrial hydrotreating conditions. Results indicate that under HDS conditions, $CoMo/SiO_2$ still presents a four times higher average stacking value than $CoMo/Al_2O_3$ with almost exclusively single slabs. Fresh $CoMo/SiO_2$ catalysts before any test were found to present an average stacking value 25% higher than $CoMo/Al_2O_3$. These results reveal that possible modifications under HDS conditions can lead to erroneous conclusions if compared to an analysis based only on fresh catalysts. While multilayered entities could be found on the freshly sulfided $CoMo/Al_2O_3$, almost only single-slab moieties were observed on the DBT tested $CoMo/Al_2O_3$. As expected, on a weakly interacting support like silica, multistacked slabs are still detected. However, in any case, the full scattering analysis of the relative proportions of stacked and unstacked particles clearly underlines that stacked layers represent only a minor percentage for supported catalysts and this fact should be kept in mind when considering the real dispersion of the active phase. Finally, one should note that the model DBT-tested $CoMo/Al_2O_3$ catalyst appears less stacked than the commercial CoMo D-1W and D-1M samples. However, the commercial $CoMo/Al_2O_3$ catalysts contain phosphorus as a doping additive. Therefore, our results confirm that phosphorus doping increases the stacking height as already observed in previous studies [41,42].

The lateral growth evolution results suggest that the HDS test did not induce any substantial change in lateral growth of MoS_2 particles since D_{110} values hardly changed during the HDS test (from 44 to 46 Å for $CoMo/Al_2O_3$ and from 64 to 66 Å for $CoMo/SiO_2$). However, longer times of use in industrial conditions reveal an evolution of lateral dimensions. Lateral D_{110} values increased by 15–20% between D-1W and D-4Y samples. This result suggests that lateral growth is a slower process than destacking. The increase in lateral dimensions should be considered when explaining the decrease in activity between D-1W and D-4Y since a larger lateral dimension would result in a lower proportion of Mo edge sites in comparison to the total number of Mo atoms per crystallite. However, another parameter should be considered. Indeed, coke formation could be particularly harmful for D-4Y samples submitted to a blend feedstock containing 20% of LCO known to present a high aromatics content [43].

When HDS conditions were applied, particles for the model $CoMo/Al_2O_3$ catalyst remained more dispersed than on $CoMo/SiO_2$ ($D_{110} = 46$ Å vs 66 Å, $\bar{n} = 1.0$ vs 4.0, ratio stacked/unstacked layers = 2/98 vs 7/93). The higher lateral dispersion of $CoMo/Al_2O_3$ could partly explain the 60% higher activity of this catalyst compared to $CoMo/SiO_2$. However, $CoMo/SiO_2$ presents a higher proportion of CoMo multilayered species. These species called "type II" by Candia et al. [35] are expected to be more active than single-layered species called "type I." Indeed, even if stacked particles represent only 7% of all the particles for this catalyst, the high average value for these stacked layers ($\bar{n} = 4.0$) would correspond to about 20% of type II species. This higher amount of multilayered sites would at least partly reduce the difference in activity between $CoMo/Al_2O_3$ and $CoMo/SiO_2$, but this is not the case here. In fact, under the liquid-phase HDS conditions, multilayered type II species do not seem more active than single layers. This result is in agreement with previous studies showing contradictory results about the respective intrinsic HDS activity of multilayered and single-layered active sites in gas-phase or liquid-phase HDS reactions. Indeed, in the gas-phase HDS of thiophene, single-layered species were found to be less active than multilayered entities [35] whereas under the liquid-phase HDS of DBT, multilayered type II species did not have higher activity compared to single layered type I sites [44].

The main cause for the destacking process observed both for model catalysts under DBT HDS test or for commercial catalysts used in industrial conditions is related to the high pressure applied during the hydrotreating conditions. Indeed, fresh model catalysts before the HDS test have been sulfided at atmospheric pressure only under an H_2S/H_2 gas mixture. Peng et al. have reported a similar pressure–crystallization effect with stacking decreasing with increasing pressure inside the reactor during the hydrothermal synthesis of MoS_2 in an autoclave [45]. In the present study, a strong decrease in stacking was observed even after only 10 h in a DBT HDS catalytic test. A similar decrease in stacking from $\bar{n} = 1.7$ to $\bar{n} = 1.0$ was found between the D-1M and the D-4Y samples. This decrease in stacking is concomitant with an increase in pressure from 5.5 MPa for D-1M to 7.8 MPa for D-4Y. However, comparison between the D-1W and the D-1M samples operating at the same pressure (5.5 MPa) reveals a slighter but still significant decrease in stacking from $\bar{n} = 1.7$ to $\bar{n} = 1.5$. This suggests that other experimental parameters of the HDS process, mainly the hydrocarbon pressure or concentration, can contribute to the destacking effect. In agreement with the model proposed by Peng et al. [45] under high pressure, the formation of multilayered stacks through van der Waals forces seems counterbalanced by the strong interaction of adsorbed substances (here, hydrocarbon molecules) favoring the stabilization of single MoS_2 layers. This destacking effect seems accentuated if a strongly interacting support is present. This result

would also corroborate a recent study by Glasson et al. showing that less stacked $CoMo/Al_2O_3$ catalysts can be obtained if pretreated with gas oil or coleseed oil [11]. Their treatment at atmospheric pressure shows by itself than hydrocarbons are able to favor a destacking process. However, applying high pressure will favor the stabilization effect by increasing the interaction between hydrocarbons and MoS_2 single layers.

The higher signal to noise ratio of the synchrotron source also revealed the presence of Co_9S_8 as a secondary phase early in the commercial catalysts' life. The Co_9S_8 peaks diminished in intensity during steady-state working conditions in the D-1W and D-1M samples in an HDS pilot plant. The D-4Y sample presented a much attenuated intensity for the Co_9S_8 phase but also a weak signal due to the Co metallic phase. Therefore, X-ray synchrotron analysis confirms the presence of an initial Co_9S_8 phase in low proportion, which tends to be reduced into Co^0 under severe hydrotreating conditions.

5. Conclusion

The advantage of using the synchrotron X-ray radiation is clearly demonstrated compared to highly ambiguous "in-house" X-ray diffraction. We were able to determine the ratio of stacked to unstacked MoS_2 in supported industrial catalysts. It appears that the commercial catalysts contain more than 90% single layers. HRTEM studies reported an average stacking height of 3–4 layers, but badly misinterpret the properties of the catalyst because hardly 10% of the active phase has the orientation and thickness adequate to be imaged by the microscope. Synchrotron X-ray-scattering studies of cobalt-promoted silica- or alumina-supported CoMo catalysts has led to the following conclusions:

1. The importance of the support interaction with the active phase is confirmed. Strongly interacting supports favor the formation of single MoS_2 layers. On the other hand, weakly interacting supports lead to reorganization into multilayered slabs. However, in any case, the proportion of stacked particles remains low.
2. Hydrotreating conditions induce a destacking process in model and commercial catalysts. In this respect, commercial $CoMo/Al_2O_3$ catalysts that have been run for long periods of time under high pressure conditions tend to destack. The destacking of the layers result from a combination of carbonaceous deposits and high pressure during the reaction conditions.
3. The higher signal to noise ratio of the synchrotron source also revealed the presence of Co_9S_8 as a secondary phase early in the commercial catalysts' life. The Co_9S_8 peaks diminished in intensity during steady-state working conditions and a weak signal of the Co metallic phase is observed. Furthermore, HRTEM micrographs support this finding. Therefore, X-ray synchrotron analysis confirms the presence of an initial Co_9S_8 phase in low proportion, which tends to be reduced into Co^0 under severe hydrotreating conditions.

This study emphasizes the importance of in situ characterizing catalysts to determine changes occurring during HDS conditions or if impossible to characterize these solids before and after HDS test to evaluate the real nature of the active phase when reaction conditions are applied. The stacking evolution observed clears up uncertainty in the literature and promises to generate new understanding of structure/function relations in commercial catalysts.

Acknowledgments

Portions of this research were carried out at the Stanford synchrotron Radiation Laboratory, a national user facility operated by Stanford University on behalf of the US Department of Energy, Office of Basic Energy Sciences. The wonderful staff at the SSRL is gratefully acknowledged. We thank the US Department of Energy Gateway Program and the Robert A. Welch Foundation for financial support. We also acknowledge J.L. Elechiguerra for his valuable assistance. We thank the Instituto Mexicano del Petroleo for providing us the spent catalysts for this study.

References

[1] R.R. Chianelli, M. Daage, M. Ledoux, Adv. Catal. 40 (1994) 177.
[2] J.H. Voorhoeve, J.C.M. Stuiver, J. Catal. 23 (1971) 243.
[3] A.L. Farragher, P. Cossee, in: J.W. Hightower (Ed.), Proceedings of the 5th International Congress on Catalysis, North-Holland, Amsterdam, 1973, p. 1301.
[4] G. Hagenbach, P. Courty, B. Delmon, J. Catal. 31 (1973) 264.
[5] C. Wivel, R. Candia, B.S. Clausen, S. Mørup, H. Topsøe, J. Catal. 68 (1981) 453.
[6] J.V. Lauritsen, S. Helveg, E. Lægsgaard, I. Stensgaard, B.S. Clausen, H. Topsøe, F. Besenbacher, J. Catal. 197 (2001) 1.
[7] P. Raybaud, J. Hafner, G. Kresse, S. Kasztelan, H. Toulhoat, J. Catal. 190 (2000) 128.
[8] H. Schweiger, P. Raybaud, H. Toulhoat, J. Catal. 212 (2002) 33.
[9] R.R. Chianelli, G. Berhault, P. Raybaud, S. Kasztelan, J. Hafner, H. Toulhoat, Appl. Catal. A 227 (2002) 83.
[10] P. Afanasiev, G.F. Xia, G. Berhault, B. Jouguet, M. Lacroix, Chem. Mater. 11 (1999) 3216.
[11] C. Glasson, C. Geantet, M. Lacroix, F. Labruyère, P. Dufresne, J. Catal. 212 (2002) 76.
[12] G. Berhault, A. Mehta, A. Pavel, J. Yang, L. Rendon, M.J. Yácaman, L. Cota, A. Duarte, R.R. Chianelli, J. Catal. 198 (2001) 9.
[13] G. Berhault, L. Cota, A. Duarte, A. Mehta, R.R. Chianelli, Catal. Lett. 78 (2002) 81.
[14] G. Alonso, V. Petranovskii, M. Del Valle, J. Cruz-Reyes, A. Licea-Claverie, S. Fuentes, Appl. Catal. A 197 (2000) 87.
[15] V. Schwartz, T.V. Da Silva, S.T. Oyama, J. Mol. Catal. A: Chem. 163 (2000) 251.
[16] R. Murray, B.L. Evans, J. Appl. Crystallogr. 12 (1979) 312.
[17] K.I. Tanaka, Adv. Catal. 33 (1985) 99.
[18] M. Salmeron, G.A. Somorjai, A. Wold, R.R. Chianelli, K.S. Liang, Chem. Phys. Lett. 90 (1983) 105.

[19] M. Daage, R.R. Chianelli, J. Catal. 149 (1994) 414.
[20] R.R. Chianelli, E.B. Prestridge, T.A. Pecoraro, J.P. DeNeufville, Science 203 (1979) 1105.
[21] C. Calais, N. Matsubayashi, C. Geantet, Y. Yoshimura, H. Shimada, A. Nishijima, M. Lacroix, M. Breysse, J. Catal. 174 (1998) 130.
[22] R.R. Chianelli, M. Daage, in: M.L. Occelli, R.G. Anthony (Eds.), Hydrotreating Catalysts—Preparation, Characterization and Performance, Elsevier, Amsterdam, 1989, p. 120.
[23] Y. Okamoto, Catal. Today 39 (1997) 45.
[24] T. Shido, R. Prins, J. Phys. Chem. B 102 (1998) 8426.
[25] G. Plazenet, S. Cristol, J.-F. Paul, E. Payen, J. Lynch, Phys. Chem. Chem. Phys. 3 (2001) 246.
[26] D.I. Kochubey, V.P. Babenko, React. Kinet. Catal. Lett. 77 (2002) 237.
[27] J. Van Doorn, J.A. Moulijn, G. Djéga-Mariadassou, Appl. Catal. 63 (1990) 77.
[28] R.R. Chianelli, A.F. Ruppert, M.J. Yácaman, A.V. Zavala, Catal. Today 23 (1995) 269.
[29] R.R. Chianelli, Int. Rev. Phys. Chem. 2 (1982) 127.
[30] K.S. Liang, R.R. Chianelli, F.Z. Chien, S.C. Moss, J. Non-Cryst. Solids 79 (1986) 251.
[31] S.S. Pollack, J.V. Sanders, R.E. Tischer, Appl. Catal. 8 (1983) 383.
[32] F. Luck, Bull. Soc. Chim. Belg. 100 (1991) 781.
[33] M. Breysse, J.L. Portefaix, M. Vrinat, Catal. Today 10 (1991) 489.
[34] H. Topsøe, J. Catal. 216 (2003) 155.
[35] R. Candia, O. Sorensen, J. Villadsen, N.Y. Topsøe, B.S. Clausen, H. Topsøe, Bull. Soc. Chim. Belg. 93 (1984) 763.
[36] S. Eijsbouts, J.J.L. Heinerman, H.J.W. Elzerman, Appl. Catal. A 105 (1993) 69.
[37] S. Eijsbouts, Y. Inoue, Sci. Technol. Catal. 76 (1994) 429.
[38] J.G. Weissman, J.C. Edwards, Appl. Catal. A 142 (1996) 289.
[39] Y. Yokoyama, N. Ishikawa, K. Nakanishi, K. Satoh, A. Nishijima, H. Shimada, N. Matsubayashi, M. Nomura, Catal. Today 29 (1996) 261.
[40] Y. Ni, J. Zang, Y. Zhao, J. Wang, Stud. Surf. Sci. Catal. 88 (1994) 401.
[41] J. Ramírez, V.N. Castaño, C. Leclercq, A. López-Agudo, Appl. Catal. A 83 (1992) 251.
[42] R. Hubaut, O. Poulet, S. Kasztelan, E. Payen, J. Grimblot, in: M.L. Occelli, R.R. Chianelli (Eds.), Hydrotreating Technology for Pollution Control, Dekker, New York, 1996, p. 115.
[43] J. Chen, M. Te, H. Yang, Z. Ring, Petr. Sci. Technol. 21 (2003) 911.
[44] H.R. Reinhoudt, C.H.M. Boons, A.D. van Langeveld, J.A.R. van Veen, S.T. Sie, J.A. Moulijn, Appl. Catal. A 207 (2001) 25.
[45] Y. Peng, Z. Meng, C. Zhong, J. Lu, W. Yu, Z. Yang, Y. Qian, J. Solid State Chem. 159 (2001) 170.